ACS APPLIED MATERIALS & INTERFACES

www.acsami.org Research Article

Identification of a Direct-Acting Antiviral Agent Targeting RNA Helicase via a Graphene Oxide Nanobiosensor

Jungho Kim, Se-Jin Park, Jisang Park, Hojeong Shin, Yong-Suk Jang, Jae-Sung Woo, and Dal-Hee Min*

Cite This: *ACS Appl. Mater. Interfaces* 2021, 13, 25715−25726 Read Online

ACCESS | Metrics & More | Article Recommendations | Supporting Information

ABSTRACT: Dengue virus (DENV), an arbovirus transmitted by mosquitoes, causes infectious diseases such as dengue fever, dengue hemorrhagic fever, and dengue shock syndrome. Despite the dangers posed by DENV, there are no approved antiviral drugs for treatment of DENV infection. Considering the potential for a global dengue outbreak, rapid development of antiviral agents against DENV infections is crucial as a preemptive measure; thus, the selection of apparent drug targets, such as the viral enzymes involved in the viral life cycle, is recommended. Helicase, a potential drug target in DENV, is a crucial viral enzyme that unwinds double-stranded viral RNA, releasing single-stranded RNA genomes during viral replication. Therefore, an inhibitor of helicase activity could serve as a direct-acting antiviral agent. Here, we introduce an RNA helicase assay based on graphene oxide, which enables fluorescence-based analysis of RNA substrate-specific helicase enzyme activity. This assay demonstrated high reliability and ability for high-throughput screening, identifying a new helicase inhibitor candidate, micafungin (MCFG), from an FDA-approved drug library. As a direct-acting antiviral agent targeting RNA helicase, MCFG inhibits DENV proliferation in cells and an animal model. Notably, *in vivo*, MCFG treatment reduced viremia, inflammatory cytokine levels, and viral loads in several tissues and improved survival rates by up to 40% in a lethal mouse model. Therefore, we suggest MCFG as a potential direct-acting antiviral drug candidate.

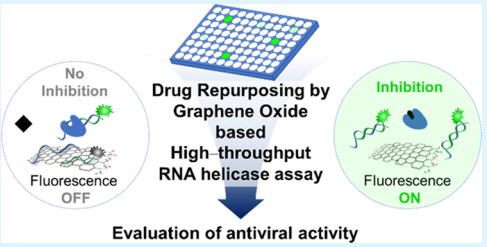

KEYWORDS: *antiviral agent, biosensor, dengue virus, graphene oxide, high-throughput drug screening*

INTRODUCTION

Viral infectious diseases pose a significant threat to human health.[1] However, vaccine development and improvements in hygiene have significantly contributed to the partial suppression of emerging viral diseases. Nevertheless, little success has been achieved in controlling viral epidemics, as evidenced by the outbreak of severe acute respiratory syndrome in 2002, Ebola in 2013, middle-Eastern respiratory syndrome and Zika in 2015,[2] and COVID 19.[3,4]

Dengue fever (DF) is a prominent infectious viral disease, with 50 million infections reported annually, including 500,000 hospitalizations for dengue hemorrhagic fever or dengue shock syndrome, with a fatality rate of 2.5%. The causative agent of DF is the dengue virus (DENV), a mosquito-borne single positive-stranded RNA virus of the family Flaviviridae.[5,6] Given that advances in transportation systems have accelerated the spread of DENV globally, it has now been disseminated to more than 100 countries in Southeast Asia, the western Pacific, Europe, and North and South Americas.[5,6] Nevertheless, there are limited treatments for DENV such as supportive care, with no approved drugs.[7]

Nucleoside analogs and chemical drugs targeting host enzymes have been previously investigated.[8−10] However, the harmful adverse effects of these strategies, such as metabolic disorders, hindered the development of antiviral agents;[11,12] for example, Celgosivir, which targets the host enzyme α-glucosidase, is recommended for the short-term treatment of DENV owing to its intrinsic toxicity,[13] while NITD008, a nucleoside analog, did not proceed to clinical trials owing to the significant side effects observed during preclinical studies.[14] The development of direct-acting antiviral agents (DAAs) can be an effective strategy to overcome the limitations of conventional antiviral drug development methodologies. DAAs are a novel class of drugs that target specific stages in the viral life cycle; the working mechanisms of these drugs provide them with high eradication rates and excellent safety profiles.[15,16]

One of the major challenges in antiviral discovery is its tedious and time-consuming stages, which is not enough to prevent the rapid spread of the virus. Drug repurposing has been proposed as a breakthrough to accelerate the drug development process. The concept of drug repurposing is to assign approved drugs to new indications. Thus, repurposed drugs can easily enter clinical trials and may even bypass phase I clinical studies, shortening the time required for a potential

Received: March 11, 2021
Accepted: May 17, 2021
Published: May 26, 2021

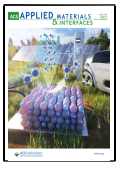

https://doi.org/10.1021/acsami.1c04641
ACS Appl. Mater. Interfaces 2021, 13, 25715−25726

antiviral agent to reach clinical applications.[17,18] Therefore, the development of DAAs through repurposing can be an effective approach to discover potential antiviral candidates and reduce their developmental period.

The main targets of DAAs are virus-encoded proteins that are crucial for viral replication, such as a helicase, which is involved in the viral replication cycle and unwinds double-stranded RNA to release single-stranded RNA viral genomes.[19−22] To discover DAAs targeting the helicase, a number of high-throughput screening (HTS) strategies have been introduced, based on various assays, including nucleic acid binding, ATPase, and thermo-shift assays.[23−26] However, since these assays detect binding with nucleic acid, interference with hydrolysis or binding of ATP, and interactions between proteins and drugs, rather than whole unwinding activities, they remain limited. Therefore, it is essential to screen drugs against the enzymes' activities, which can provide various inhibition sites. Conventional unwinding activity assays are limited; for example, the conventional gel-shift assay is labor-intensive and time-consuming. The molecular beacon assay is another conventional method with high potential; however, there have been several concerns regarding its low selectivity due to signal interference. Therefore, these conventional methods are not suitable for developing DAAs targeting the helicase.[23,27]

Previously, we described a new and simple helicase assay, graphene oxide (GO)-based helicase assay, that produced robust results.[28,29] Since GO has a high affinity for nucleobases and fluorescence-quenching ability, it enables convenient fluorescence-based analysis. However, this assay was designed using a thoroughly studied viral helicase model, the hepatitis C virus (HCV) NS3, which exhibits high *in vitro* unwinding activity on the DNA substrate despite the genome of HCV being a single-stranded RNA.[30−32] Considering that typical viral RNA helicases, including the DENV helicase, recognize RNA as a substrate,[33,34] improvements are required to utilize this system as a general RNA helicase activity assay.

Here, we present an advanced GO-based helicase assay, referred to as the RNA helicase assay based on GO (RheGO) (Scheme 1). We demonstrated that RheGO, a fluorescence-based assay, provides robust results and is suitable for antiviral drug screening. Using RheGO, we performed high-throughput screening against a Food and Drug administration (FDA)-approved drug library and identified micafungin (MCFG), an antifungal agent, as a potent DENV helicase inhibitor. Moreover, MCFG showed significant antiviral efficacy in both cells and animal models. MCFG treatment significantly inhibited DENV proliferation in Vero E6 cells. Using dengue mouse models, we found that MCFG also decreased viremia, inflammatory cytokine levels, and viral loads in tissues as well as increased the survival rate. Collectively, we suggest that MCFG can be a promising DAA candidate against DENV.

Scheme 1. Research Scheme of RheGO Based High-Throughput Viral Enzyme Inhibitor Screening

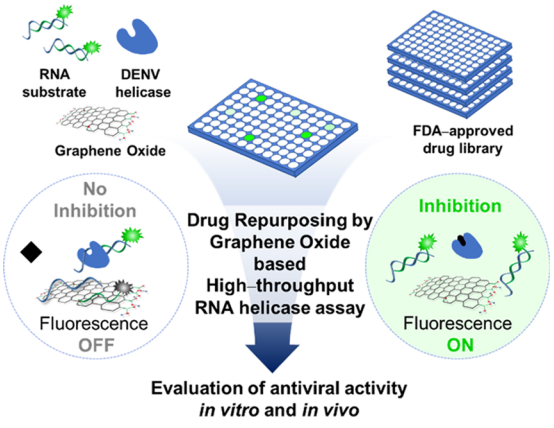

RESULTS

Evaluation of *In Vitro* Unwinding Activity of the DENV Helicase. Before establishing the GO-based helicase assay, we examined the *in vitro* activity of the DENV helicase prepared from NS3 by cloning and expressing the enzyme in *E. coli* (Figure S1A). Unlike the HCV helicase, the DENV helicase exhibits poor *in vitro* unwinding activity on the dsDNA substrate. Therefore, it is essential to obtain an optimal nucleic acid substrate to improve the unwinding activity of the DENV helicase. As demonstrated previously, when DENV helicase binds to RNA as the major strand, excellent *in vitro* unwinding activity was observed, regardless of the type of the minor strand, i.e., DNA or RNA. Therefore, we prepared a helicase substrate consisting of an RNA as a major strand and a fluorescent dye-modified DNA minor strand (Figure S1B).

With the prepared DENV helicase and substrate, we performed a conventional gel-shift assay (Figure S1C) and demonstrated that the presence of a helicase in the reaction mixture generated ssDNA; the helicase released ssDNA when ATP, the energy source for the helicase, was added to the reaction mixture (Figure S1C lanes 5 and 6). Moreover, the amount of ssDNA was directly proportional to the concentration of the helicase (Figure S1C lanes 6−8).

Development of GO-Based RNA Helicase Assay (RheGO). Based on the data obtained from previous experiments, we developed a fluorescence-based DENV helicase assay platform, RheGO, consisting of RNA substrate and GO. RheGO is based on the physicochemical properties of GO, which has a hexagonal sp^2 carbon domain and oxygen-containing chemical functional groups, thus enabling GO to interact strongly with aromatic molecules, including nucleobases and chemical dyes, via $\pi-\pi$ interactions and hydrogen bonds. GO can also quench fluorescence from chemical dyes via fluorescence resonance energy transfer.[35,36] Owing to these properties, we hypothesized that GO is utilized in RheGO as a scavenger of single-stranded nucleic acids with exposed nucleobases and as a quencher of fluorescent dyes. Thus, using fluorescent dye-modified double-stranded nucleic acid substrates and GO, the helicase activity (i.e., unwinding of double-stranded substrate into single strands) could be examined using fluorescence signals.

As one of the major components of RheGO, GO was synthesized using the modified Hummers' method.[37] The single-layered structure of the GO sheet was analyzed using atomic force microscopy (AFM) (Figure S2A). The height profile displayed GO sheets with a thickness of approximately 1 nm. Fourier-transform infrared spectroscopy (Figure S2B) revealed C=O and C−O stretching peaks at 1728 and 1049 cm^{-1}, respectively, indicating oxygen-containing functional groups. In addition, Raman spectroscopy detected a D peak attributed to structural disorder and a G peak related to the ordered sp^2 domain at 1350 and 1605 cm^{-1}, respectively (Figure S2C).

https://doi.org/10.1021/acsami.1c04641
ACS Appl. Mater. Interfaces 2021, 13, 25715−25726

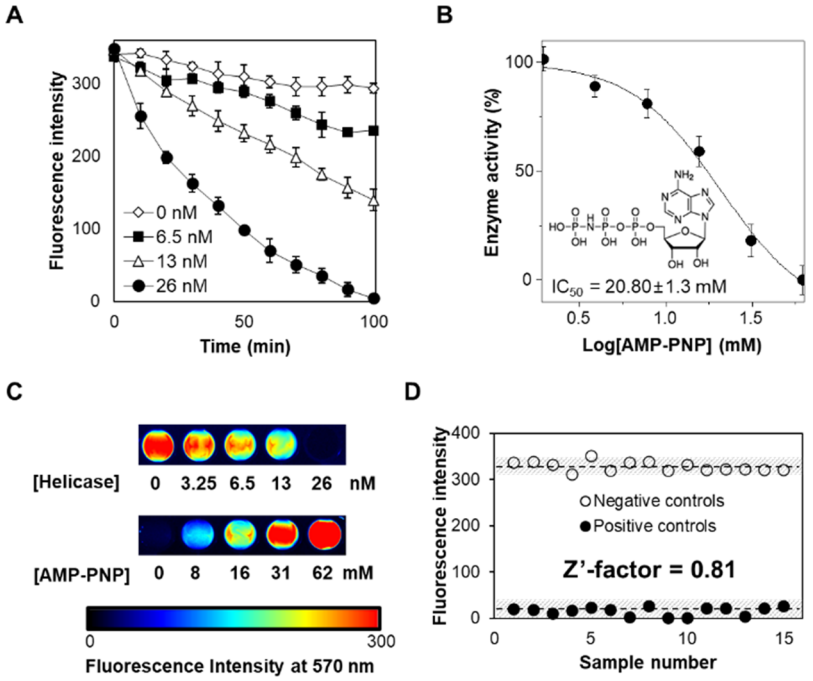

Figure 1. Performance validation of RheGO. (A) Concentration-dependent monitoring of the helicase activity by RheGO. (B) Dose-dependent inhibition of the helicase with various concentrations of AMP-PNP added into RheGO. (C) Fluorescence images obtained from a concentration-dependent assay. Row 1: helicase addition; row 2: AMP-PNP addition. (D) Z′-factor analysis showing the reliability of the assay. Bars in all graphs indicate the ±SEM.

Next, we performed RheGO and found that the fluorescence signal changed, showing an emission at 570 nm (Figure 1A). The negative control (0 nM) showed slightly decreased fluorescence signals; however, a plateau with high signal was soon reached. The addition of helicase decreased the fluorescence signal over time, and the rate of signal reduction increased in a helicase concentration-dependent manner. The concentration-dependent result correlated with the gel-shift assay outcomes (Figure S1C lanes 6−8). Using RheGO, we found a significant difference in fluorescence intensity between the reaction mixtures with and without 26 nM helicase within 50 min.

Additionally, we determine whether RheGO could detect enzyme inhibition when an enzyme inhibitor is added. Given that ATP is the energy source for helicase, adenylyl-imidodiphosphate (AMP-PNP), a non-hydrolysable ATP analog, can serve as a model inhibitor of helicase activity. Therefore, we performed RheGO with the addition of various concentrations of AMP-PNP (Figure 1B) and observed a dose−response inhibition effect. We calculated the half-inhibitory concentration (IC_{50}) value to be approximately 20 mM.

Finally, to verify the feasibility of RheGO as an inhibitor screening platform, we examined its robustness. First, we obtained fluorescence images of multiple reaction mixtures. In the first row, the samples were prepared by varying the helicase concentrations in a 96-well plate. In the second row, the samples with various AMP-PNP concentrations were arranged. As expected, the fluorescence images showed that the fluorescence intensity of each well reflected the helicase activity and inhibitory activity quantitatively (Figure 1C). Meanwhile, as a statistical value that warrants the assay proposing high-throughput screening, the Z′-factor is commonly used.[38] A Z′-factor value from 0.5 to 1 indicates that the assay is highly reliable. Our calculations showed that the Z′-factor of RheGO was 0.81 (Figure 1C), indicating that RheGO is suitable for high-throughput screening.

Screening Helicase Inhibitor from an FDA-Approved Drug Library. We have thus far showed that RheGO can be used as a high-throughput screening platform for discovering DENV helicase inhibitors. Using RheGO, we performed high-throughput inhibitor screening against FDA-approved drug library consisting of 1443 compounds. The brief procedures and results of this strategy, referred to as drug repurposing, are as follows: First, to narrow down the range of inhibitor candidates rapidly, primary screening was executed (Figure 2A). We added 100 μM of each compound to RheGO plates in the primary screening step and then identified 41 compounds showing an inhibitory effect that exceeded 50% (Figure 2C).

In addition, to remove false signals generated by the interference between the compounds and other components apart from the helicase, we used a counter-screening process (Figure 2B). The counter-screening process involved a single strand substrate instead of the duplex substrate. In such a circumstance, the RheGO system would always exhibit the quenched fluorescence. Compounds, which disrupted the ordinary quenching, were screened out. Throughout the counter-screening process, six valid inhibitor candidates were selected from the library. Using the ratio between the half maximal inhibitory and cytotoxicity concentrations, we selected micafungin (MCFG), which showed the greatest suppression efficacy with an IC_{50} value of approximately 5 μM and the lowest cytotoxicity over 250 μM, as a hit compound (Figure 2D).

The Hit Compound Micafungin Showed *In Vitro* Antiviral Activity in a Cell-Based Assay. Owing to the inhibitory effect of MCFG against the DENV helicase, we expected that MCFG would exhibit antiviral activity in cell-

https://doi.org/10.1021/acsami.1c04641
ACS Appl. Mater. Interfaces 2021, 13, 25715−25726

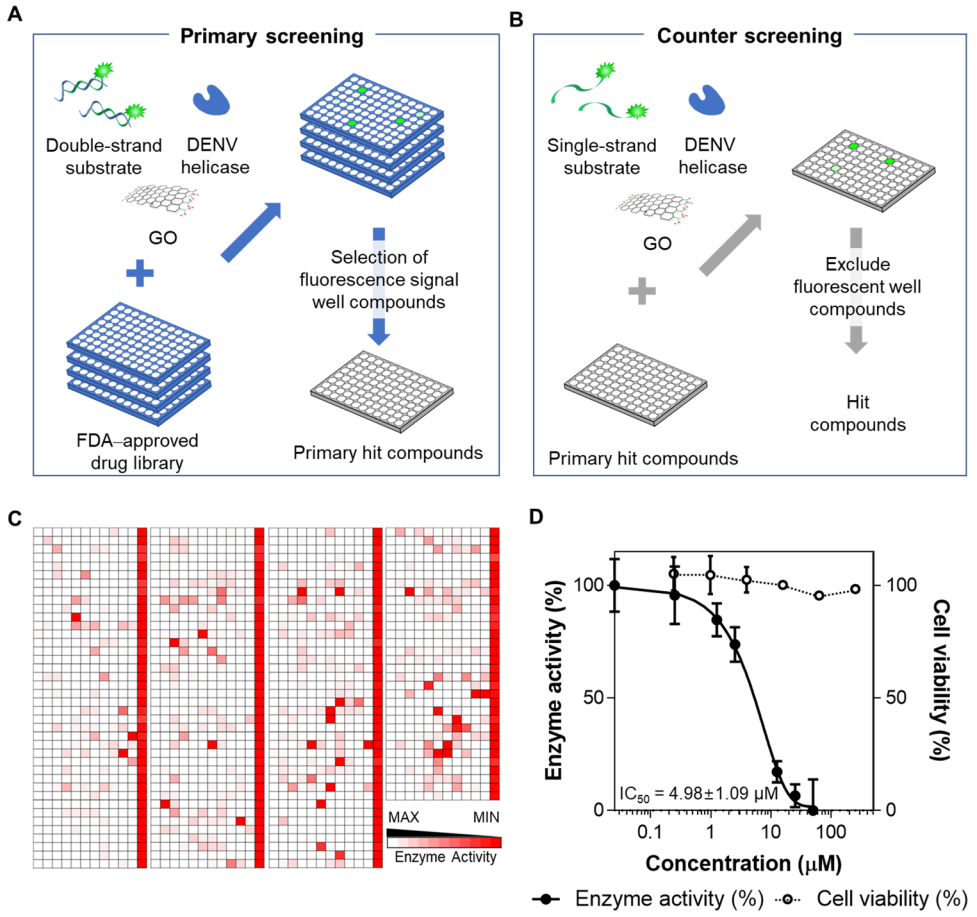

Figure 2. Strategy of drug repurposing and discovery of a DENV helicase inhibitor based on RheGO. (A) Scheme for primary screening with RheGO. (B) Scheme of a counter-screening strategy to detect false-positive compounds, and (C) primary screening against 1443 FDA-approved chemical compounds. Each plate contained replicated negative and positive controls in the first and last columns, respectively. (D) Dose-dependent inhibition of the dengue helicase and cell (Vero E6) viability after treatment with various concentrations of MCFG. Calculated IC_{50} value for the hit compound is also shown. Bars in the graph indicate the ±SEM.

based assays as well. Before the MCFG treatment to cells, the cytotoxicity of MCFG was first evaluated (Figure 3A). MCFG did not show cytotoxicity at doses up to 300 μM in Vero E6 cells. Subsequently, to prove the antiviral effect of MCFG, a focus reduction assay was conducted (Figure 3B). We inoculated 100 focus forming units (FFU) of dengue virus serotype 2 (DENV2) with various MCFG concentrations into Vero E6 cells and then incubated them for 48 h. The formation of the viral focus was inhibited in a dose-responsive manner with a half-maximal effective concentration (EC_{50}) of approximately 46 μM. Additionally, we analyzed the amount of viral RNA in the infected cells to confirm the MCFG antiviral efficacy (Figure 3C). After DENV2 was inoculated into Vero E6 cells at a multiplicity of infection of 0.1, MCFG was added at various concentrations. Real-time PCR analysis showed that the amount of viral RNA decreased as the MCFG concentration increased. At 38 μM MCFG treatment, approximately 50% reduction of viral RNA in cells was noted. Furthermore, immunofluorescence images revealed that the DENV antigen declined in a dose-responsive manner (Figure 3D).

To determine whether MCFG has similar antiviral activity on a human cell line, we performed the same experiments in Huh-7 cells, a human hepatoma-derived cell line. Based on the results of the experiments with Vero E6 cells, Huh-7 cells were treated with MCFG up to the maximum dosing concentration of 150 μM for 48 h; no substantial cytotoxicity was observed (Figure 3E). Furthermore, the expression level of viral RNA in DENV2-infected Huh-7 cells was correlated with the MCFG concentration (Figure 3E). These results were further confirmed by immunofluorescence images, demonstrating a similar tendency to the effects on Vero E6 cells (Figure 3F).

MCFG Showed *In Vivo* Antiviral Efficacy. As MCFG showed an antiviral effect *in vitro*, we subsequently evaluated its antiviral efficacy in an animal model using the AG129 mouse strain, which is a type I & II interferon receptor knockout transgenic mouse, which is commonly used to build the DENV-infected model. AG129 mouse is susceptible not only to non-adapted DENV but also to clinical strains of DENV.[39,40] We previously reported that intraperitoneal (i.p.) injection of a 1×10^7 FFU/mouse dose of DENV2 resulted in characteristic symptoms of DENV infection and increased mortality in infected mice.[41] Based on this report, we established a DENV infection mouse model.

We then assessed changes in pathological signs and symptoms following treatment with MCFG *in vivo*. Initially, we confirmed the peak viremia change according to the drug treatment (Figure 4A). At a dose of 75 mg/kg once a day, there was a significant (87%) decrease in the peak viremia level ($p < 0.05$), indicating that MCFG could reduce the viral load

https://doi.org/10.1021/acsami.1c04641
ACS Appl. Mater. Interfaces 2021, 13, 25715−25726

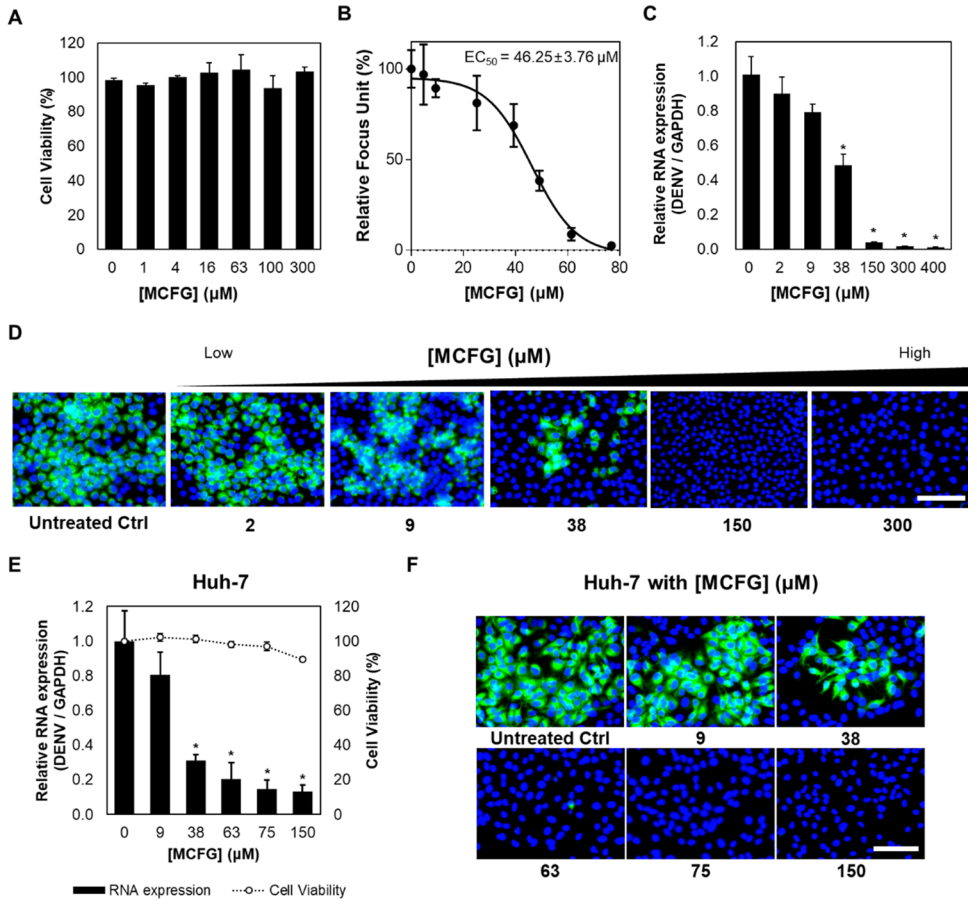

Figure 3. Cell-based antiviral evaluation of MCFG. (A) Cell (Vero E6) viability after treatment with various concentrations of MCFG (n = 5). (B) Dose-dependent inhibition of DENV replication and the calculated EC_{50} value for MCFG (n = 5). (C) Relative reduction of DENV RNA expression by increasing the compound (MCFG) concentration (n = 3). Statistical significance was confirmed by Student's t test; * denotes p < 0.05. (D) Immunofluorescence staining images of DENV-infected Vero E6 cells with various concentrations of MCFG. Blue, nucleus; green, DENV antigen. (E) Cell (Huh-7) viability after treatment with various concentrations of MCGF (n = 5) and the relative reduction of DENV RNA expression by increasing the compound concentration (n = 3). Statistical significance was confirmed by Student's t test. *p < 0.05. (F) Immunofluorescence staining images of DENV-infected Huh-7 cells treated with various concentrations of MCGF. Blue, nucleus; green, DENV antigen. Bars in graphs indicate the ±SEM. Scale bars represent 100 μm.

in the serum. Notably, the expression of inflammatory cytokines including tumor necrosis factor (TNF), interferon γ (IFN-γ), and interleukin 6 (IL-6) increases in mice when infected with DENV. We subsequently examined the changes in the levels of inflammatory cytokines in DENV-infected mice treated with MCFG using the same dose (Figure 4B) and found that the MCFG treatment reduced TNF, IFN-γ, and IL-6 levels by 2.0-, 2.2-, and 4.7-fold, respectively (p < 0.05).

The mice were sacrificed on day 3 post-infection, and the representative organs were collected for further analysis. First, the viral loads in the organ samples, specifically the spleen, liver, lung, large intestine, and small intestine were investigated through a real-time PCR analysis (Figure 4C). Overall, viral RNA was reduced in all the organs obtained from the MCFG-treated group. Although a significant decrease in the viral RNA was not observed in the spleen (p = 0.0873), MCFG treatment significantly reduced viral RNA in the liver, lung, large intestine, and small intestine by 2.1-, 8.7-, 4.4-, and 2.0-fold, respectively (p < 0.05). Moreover, there was a 1.5-fold reduction in the viral load in whole blood (p < 0.05). Additionally, histological alterations caused by DENV infection were examined in the liver, lung, and spleen.[40,42−44] Thus, tissue samples from the liver, lung, and spleen were fixed and embedded in paraffin. After staining the samples with hematoxylin and eosin (H&E), we assessed the specimens using an optical microscope (Figure 4E). Unlike in the phosphate buffered saline (PBS) group, focal necrosis was not observed in the MCFG treatment group in the liver. In addition, swelling of the alveolar septa in the lung due to DENV infection was diminished in the treatment group. The DENV-infected spleens showed a collapse of the boundary, referred to as the marginal zone, between white and red pulps. In the MCFG treatment group, the marginal zone was recovered.

Another pathological sign of DENV infection is splenomegaly. Hence, we investigated the weight and size of each spleen (Figure 4D and Figure S3) and found that the weight of the spleen in the DENV-infected group was significantly increased by 2.9-fold compared to that in the normal group (p < 0.05); in contrast, treatment with MCFG decreased the spleen weight by 1.4-fold compared to that in the infected mice (p < 0.05). Apart from these outcomes, increased spleen weights were also found in healthy mice treated with MCFG. Although the expansion size was smaller by 0.5-fold than that in the DENV-infected group, we confirmed, through a comparison with non-

https://doi.org/10.1021/acsami.1c04641
ACS Appl. Mater. Interfaces 2021, 13, 25715−25726

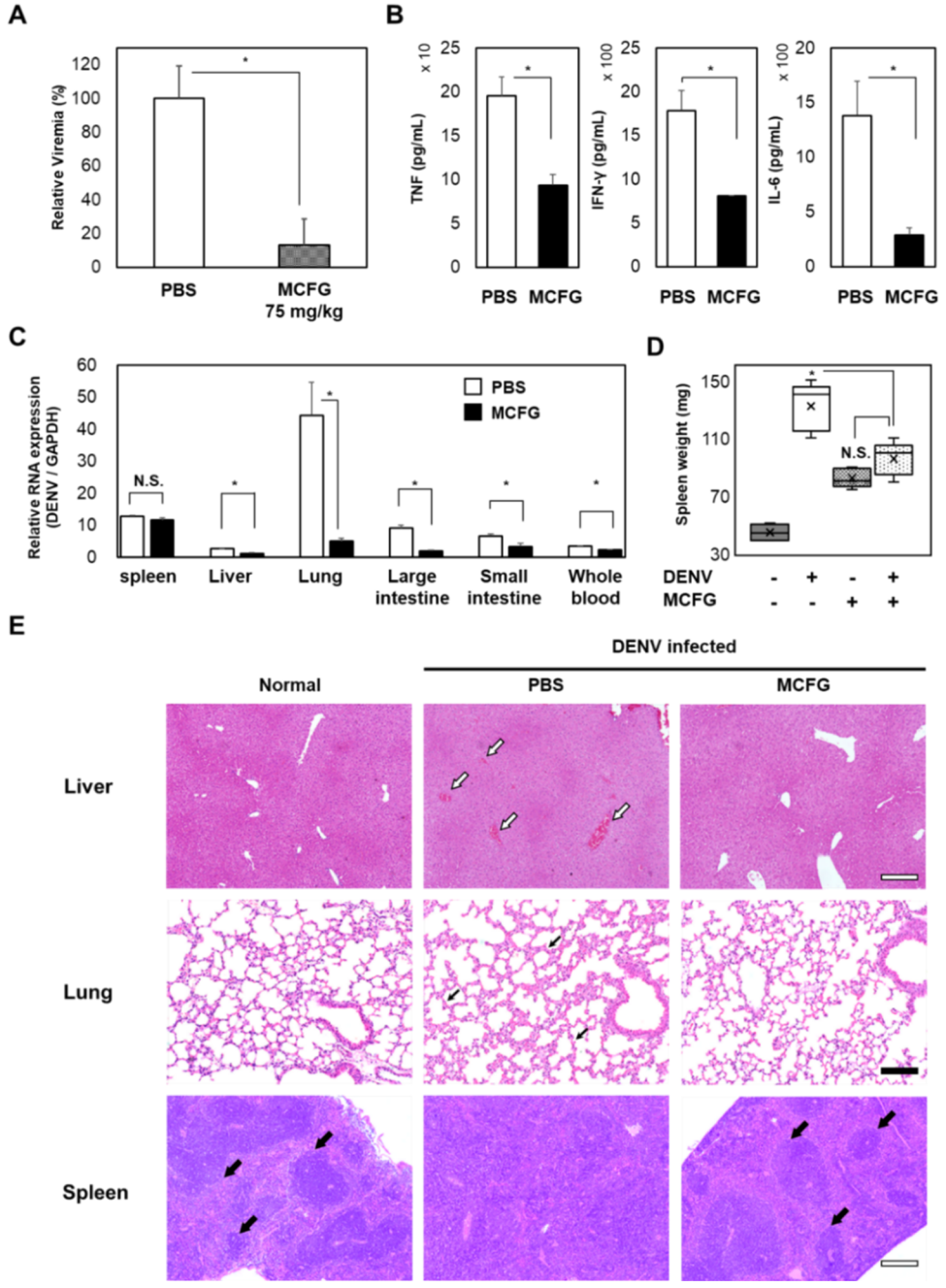

Figure 4. Antiviral activity of MCFG in DENV-infected AG129 mice. MCFG was administered at a dose of 75 mg/kg i.p. once a day in all drug treatment groups. Phosphate buffered saline (PBS) controls were also treated with a dosing schedule identical to that of the MCFG group. (A) Viremia analysis based on absolute quantification by real-time PCR (n = 3). (B) Serum cytokine analysis results from a cytometric bead array. The black bar represents the drug-treated group, and the white bar is the PBS control group (n = 5). Inflammatory cytokines including tumor necrosis factor, TNF; interferon γ. IFN-γ; interleukin 6, IL-6. (C) Analysis of viral RNA in each tissue sample by real-time PCR (n = 5). (D) Comparison of spleen weights (n = 5). (E) Hematoxylin and eosin (H&E) staining images for each experimental group. Scale bars represent 100 (black) and 200 μm (white). The white arrows indicate focal necrosis in the liver. The small black arrows represent swollen alveolar septa in the lung. The large black arrows indicate the marginal zone in the spleen. Statistical significance was confirmed by Student's t test. Bars in all graphs indicate the ±SEM. Not significant (N.S.); * for $p < 0.05$.

drug-treated healthy mice, that the spleen was indeed enlarged ($p < 0.05$).

Furthermore, DENV infection contributes to hematological changes. Notably, acute viral infection induces leukopenia and lymphopenia. Hemorrhage, a severe disease manifestation, decreases the amount of red blood cells (RBC) in the blood.[40,45] To confirm the changes in each component, we analyzed blood samples from each group (Figure S4) and found that the changes in trends were similar to those described above with regard to white blood cells (WBC), lymphocytes, and RBC in DENV-infected mice. Though the changes were not significant in the MCFG treatment group, the WBC, lymphocyte, and RBC levels increased by 1.4-, 1.2-, and 1.1-fold, respectively (p = 0.097, 0.540, and 0.262, respectively). The RBC level declined in normal mice treated with MCFG, although not significantly (p = 0.314).

https://doi.org/10.1021/acsami.1c04641
ACS Appl. Mater. Interfaces 2021, 13, 25715−25726

Given that MCFG diminished the viral load and alleviated pathological signs, we further examined whether MCFG treatment would also reduce the DENV infection-derived mortality rate. We administered a dose of 1×10^7 FFU/mouse i.p. with DENV2 into 10 mice per group. For the drug treatment group, MCFG was administered once a day at a dose of 75 mg/kg upon the start of the infection. While the infected mice without drug treatment died within 10 days, 40% of those treated with MCFG survived (Figure 5). The statistical

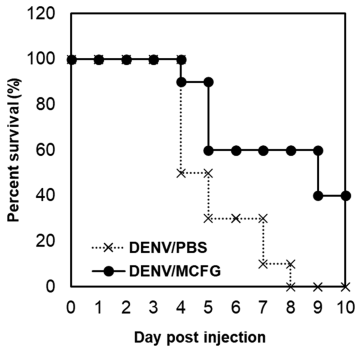

Figure 5. Survival rate of DENV-infected AG129 mice with or without MCFG treatment (n = 10). MCFG given at a dose of 75 mg/kg i.p. once a day. Statistical significance was confirmed by a log-rank test (p = 0.0046).

significance of such data was further confirmed by the Kaplan–Meier estimation model, providing the evidence for the therapeutic effect of MCFG ($p < 0.05$) (Figure S5).

DISCUSSION

In this study, we developed an RNA helicase assay based on GO, which we refer to as RheGO, which consists of GO as a cost-effective and easily prepared quencher, RNA as a crucial substrate, and DENV helicase as an active target. These constituents make RheGO a cost-effective, simple, and highly reliable assay to quantitatively measure helicase activity levels via fluorescence observations. Moreover, we demonstrate that this GO-based helicase assay has not only applied a value for a well-studied model helicase acting on a DNA substrate but also scalable application for a general RNA helicase through analysis of the DENV helicase, showing activity specific to RNA substrates.

Although there have been studies of MBHA for DENV helicase using RNA substrates,[46] RheGO has several advantages such as high reliability and reproducibility, cost-effectiveness, and simplicity by just adding GO. Moreover, RheGO provides more possibilities for discovering inhibitors than HTS based on fragment analysis of the helicase such as nucleic acid binding and ATPase assays. Thus, RheGO can be a more robust method to discover potent DAAs.

MCFG is an antifungal drug approved by the U.S. FDA in 2005 to treat candidiasis caused by a fungal infection. The chemical structure of MCFG features a cyclic hexapeptide core with a lipid sidechain. MCFG targets the 1,3-β-D-glucan synthase and inhibits the production of fungal cell walls; however, the underlying mechanism remains unknown.[47] Recent reports have suggested MCFG as an antiviral agent against enterovirus 71 and chikungunya virus.[48,49] However, these reports only evaluated the antiviral activities at the cellular level and did not reveal the antiviral mechanisms against the viruses. In contrast, our study aimed to identify the inhibitor targeting the viral RNA helicase. Based on our results, we suggest that the antiviral mechanism of MCFG against DENV is attributed to its helicase-inhibition activity. To the best of our knowledge, our study is the first to illustrate the antiviral effect of MCFG in an animal model.

In vitro, MCFG could inhibit the proliferation of DENV in cells as shown using the focus-reduction assay, analysis of relative viral RNA expression levels, and immunostaining of DENV antigen. Furthermore, similar viral inhibitor effects were found in the human cell line Huh-7, implying that the antiviral activity of MCFG does not merely affect a model cell line.

As MCFG is an FDA-approved drug, detailed information from clinical trials is available on the drug label in the FDA database, including dosing, adverse effects, and toxicity. However, there is no information regarding adverse effects in animals and thus it is difficult to interpret the unexpected results from the animal experiments in the present study. For example, the number of RBC declined in normal mice following MCFG treatment, although the difference was not statistically significant (p = 0.314). In humans, the drug label indicates that high dosing could induce hemolysis, which is supported by a clinical report.[50] Another recent report claimed that MCFG induces hemolysis by triggering cell shrinkage and cell membrane scrambling in human erythrocytes.[51] Although further investigations on the effects of MCFG to mouse blood are warranted, we suspect that this effect may be related to a similar mechanism as proposed in humans. We also observed spleen enlargement in the MCFG-treated mice; although the spleen expansion was only reduced by 0.5-fold compared with that of the DENV-infected group, it was significantly ($p < 0.05$) enlarged relative to that of untreated healthy mice. There are several potential explanations for MCFG-induced splenomegaly, including splenic congestion, hematologic malignancies, and viral infection; immune hyperplasia has also been shown to result in spleen swelling.[52−54] Considering that a previous report demonstrated the ability of MCFG to stimulate phagocytic cells and the immune response in mice,[55] we suspect that the immune-stimulation effect of MCFG is mainly responsible for the observed increase in spleen size.

Nevertheless, our *in vivo* results suggested that MCFG could be a potential treatment for DENV infection as a DAA. The rationale can be explained as follows: The significant reductions of viremia and viral load levels in the tissues of the MCFG treatment group support the contention that MCFG acts directly on DENV replication. Moreover, the viremia level can be a marker of symptom severity. For instance, in patients suffering from severe disease manifestations such as dengue hemorrhagic fever or dengue shock syndrome, viremia levels are 10-fold higher than those in patients with moderate symptoms of infection.[56,57] Here, we found that MCFG diminished viremia by approximately 8-fold, suggesting that MCFG may ameliorate disease severity. Furthermore, we observed reductions of hematocrit (HCT) and RBC levels in infected mice, indicating hemorrhage.[40,50] Treatment of DENV-infected mice with MCFG recovered HCT and RBC levels by 54 and 40%, respectively. In addition, the levels of inflammatory cytokines associated with severe manifestations were significantly reduced in DENV-infected mice treated with MCFG.[39,58] Overall, these results indicate that MCFG can alleviate hemorrhage resulting from severe cases of dengue.

https://doi.org/10.1021/acsami.1c04641
ACS Appl. Mater. Interfaces 2021, 13, 25715−25726

The potential of having a helicase inhibitor as an antiviral agent has been assessed using the HSV helicase−primase inhibitor, pritelivir, discovered using enzyme assay-based HTS.[59,60] Pritelivir dose-dependently reduced the rates of genital HSV shedding and days with lesions in a phase II clinical trial.[61] Based on these results, developments of viral helicase inhibitors targeting other viruses including HCV and DENV have been accelerated.[59] However, the inhibitor for the DENV helicase has yet to be identified.[7] Although the effect of MCFG *in vivo* showed a potential treatment strategy against dengue, further preclinical investigations are warranted prior to clinical trials. For example, the level of protection from DENV infection provided by MCFG in mice may be considered unsatisfactory. To improve the survival rate, using other animal models could be an option. Although the AG129 mouse is suitable as a dengue infection model since it shows disease symptoms similar to those in humans, this model may underestimate the therapeutic effects since it lacks an innate immune response.[62] Furthermore, the serum half-life of MCFG is shorter in mice (6.13 h) than in humans (11.3 to 20 h).[63] Considering the unfavorable pharmacokinetics of MCFG in mice, optimizing the dosing volume and schedule may improve the protection rate.

CONCLUSIONS

In summary, we utilized RheGO to identify MCFG as a promising DAA, which showed inhibitory effect against DENV proliferation both *in vitro* and *in vivo* and eventually enhanced survival rates by up to 40% in a lethal mouse model. RheGO could be used for the analysis of other RNA helicases from various RNA viruses, such as the yellow fever virus, west Nile virus, Zika virus, and SARS-CoV-2, enabling preemptive responses to viral infectious diseases through the discovery of effective antiviral agents.

METHODS AND EXPERIMENTAL SECTION

GO-Based Helicase Assay. Prepare the annealed DENV2 helicase substrate as mentioned above. Then, a solution of helicase substrate was prepared by mixing 1 μL annealed substrate stock in 75 μL 1× reaction buffer (25 mM Tris−HCl, pH 8.0,1.3 mM MgCl2, 6.25 mM NaCl, 10% glycerol).

GO solution was prepared at 2.5 μg/mL in a ATP solution (40 mM ATP, 25 mM Tris−HCl, pH 8.0, 1.3 mM MgCl2, 6.25 mM NaCl, 10% glycerol) right before use from a 1 mg/mL GO solution in distilled water. To perform the GO-based helicase assay, 15 μL of the substrate solution and 15 μL DENV2 helicase were mixed in 96-well plates. Then, 30 μL of ATP-GO solution were added to the above mixture in the 96-well plates. The final concentrations of nucleic acid substrate, ATP, GO, DENV2 helicase were 33 nM, 20 mM, 1.25 μg/mL, and 0−26 nM, respectively, in a total volume of 60 μL with a 1× reaction buffer. Next, the unwinding activity of the helicase was measured over time at 37 °C by monitoring fluorescence intensities at Ex/Em = 550 nm/570 nm (for TAMRA, substrate) with a fluorometer, SynergyMx (BioTek, UK).

Unwinding Inhibition Assay by Graphene-Oxide Based Platform. For AMP-PNP (Sigma-Aldrich, MO, USA) inhibition assay, 132 nM annealed substrate, and AMP-PNPs with various concentrations were mixed in a 1× reaction buffer. A total of 15 μL of the substrate-containing solution and 15 μL of the helicase solution were mixed by equal amounts, followed by the addition of 30 μL of the ATP-GO solution (40 mM ATP and 2.5 μg/mL GO in a 1× reaction buffer). The final concentration of the helicase was 26 nM. Fluorescence intensity measurement was performed by a fluorometer at Ex/Em = 550 nm/570 nm after 60 min incubation at 37 °C.

Measurement of the Z′-Factor. For the positive control, 15 μL of 104 nM DENV2 helicases and 15 μL of a 132 nM substrate solution were mixed in 96 well plates, followed by the transfer of 30 μL of the ATP-GO solution (40 mM ATP, 2.5 μg/mL GO in 1x reaction buffer). For the negative control, 15 μL of 104 nM boiled inactive (102 °C for 5 min) helicases and 15 μL of the 132 nM substrate solution were mixed in 96-well plates, followed by the transfer of 30 μL of the ATP-GO solution. All plates were incubated for 60 min at 37 °C. The fluorescence intensities were measured (Ex/Em = 550 nm/ 570 nm for TAMRA) (n = 15). The Z′-factor was calculated using the below equation.

$$Z' = 1 - \frac{(3\sigma_{c+} + 3\sigma_{c-})}{|\mu_{c+} - \mu_{c-}|}$$

where σ_{c+} is the standard deviation of the positive control, σ_{c-} is the standard deviation of the negative control μ_{c+} is the average of the positive control, and μ_{c-} is the average of the negative control.

Screening of the Drug Library. Basically, screening was performed by applying the same condition for the GO-based helicase assay as described above except for addition of chemical library. A total of 1443 compounds from the FDA-approved Drug Library (Selleckchem, Houston, TX, USA) were first mixed with the helicase solution at 100 μM before the addition of a mixture of ATP-GO solution and double-strand nucleic acid substrates. After the addition of the mixture of helicases and library compounds to the mixture of the substrate and ATP-GO solution, the helicase activities for double-strand nucleic acid unwinding were evaluated by measuring the fluorescence intensity at Ex/Em = 550 nm / 570 nm for TAMRA after 60 min of incubation at 37 °C using a fluorometer.

From the primary result of screening, counter screening was executed. The experimental condition of counter screening is the same with the screening procedure except that single-strand substrates were added instead of double-strand substrates.

Determination of the IC_{50}. Mixture of helicase and inhibitor compounds were prepared by mixing with a solution of 15 μL of 104 nM helicase and 0.4−4000 μM of the selected six hit compounds from the chemical library. Then, 15 μL of the substrate solution and 30 μL of the ATP-GO solution were added into 96-well plates. Fluorescence intensities were measured at Ex/Em = 550 nm/570 nm (for TAMRA) after 60 min of incubation at 37 °C. The IC_{50} values were determined by a DoseRep sigmoidal curve-fit method with OriginPro 8 (OriginLab Corporation, Northampton, MA, USA).

Cell Culture. Monkey kidney cell line (Vero E6) was kindly provided by Professor K. Ahn from the Department of Biological Science, Seoul National University. Liver carcinoma cell line (Huh-7) was purchased from American Type Culture Collection Inc. (USA). Vero E6 and Huh-7 were maintained in Dulbecco's modified minimal essential medium (DMEM) (WelGENE Inc., Seoul, Korea, LM001−09) containing 4.5 g/L D-glucose supplemented with 10% fetal bovine serum (FBS) (WelGENE Inc., Seoul, Korea, LB204−01), 100 units/mL penicillin and 100 mg/mL streptomycin in 37 °C temperature and 5% CO2 atmospheric condition unless otherwise stated.

CCK-8 Assay for the Cell Viability Test. Vero E6 and Huh-7 cells were seeded in 96 well plates with 60−70% confluency (30,000 cells/well) and incubated for overnight. After the cells were treated with various concentration of the hit compounds for 48 h, the cells were washed with phosphate buffered saline (PBS, WelGENE, Korea) solution and incubated with 10 μL of the Cell Counting Kit-8(CCK-8) (Dojindo Inc., Kumamoto, Japan, CK04) solution to analyze the active cells metabolically. CCK-8 treated cells were incubated for 1−4 h. Then, the absorbance was measured at 450 nm with a SynergyMx fluorometer.

Preparation of DENV2. DENV2 (strain KBPV-VR-29) was obtained from Korea Bank for Pathogenic Viruses (Seoul, Korea). Virus stocks were amplified in Vero E6 cells. Briefly, Vero E6 cells were inoculated with viral inoculum for 2 h at 37 °C(5 mL per T-75 flask) with shaking every 30 min, before the addition of a 15 mL medium with 2% FBS. Virus-inoculated cells were incubated at 37 °C for 6−7 days before harvesting the supernatant. After harvest, the viruses were concentrated by ultracentrifugation (Optima L-100 K

https://doi.org/10.1021/acsami.1c04641
ACS Appl. Mater. Interfaces 2021, 13, 25715−25726

with 70Ti- fixed angle rotor) at 36,000 rpm, 4 °C for 3 h. All virus stocks were stored with 20% FBS at below −70 °C before using.

Focus-Forming Unit (FFU) Assay for Viral Titer Determination. DENV2 titer was determined by infecting Vero E6 cells for 48 h with a 0.75% methylcellulose overlay and analyzing the plates for focus-forming units per mL (FFU/mL). To prepare a 0.75% methylcellulose overlay, mix 10 mL of 10× MEM (Thermo Fisher scientific, USA, 11430030), 1 mL of 100× GlutaMAX (Thermo Fisher scientific, USA, 35050061), 2.93 mL of 7.5% sodium bicarbonate (Thermo Fisher scientific, USA, 25080094), 1 mL of 100XP/S (WelGENE, Korea, LS202−02), 2 mL of FBS (WelGENE, Korea), 33.07 mL of sterile D.W., and 50 mL of sterile 1.5% methylcellulose (Sigma-Aldrich, USA).

Briefly, cells were titrated with serially diluted virus in triplicates onto a monolayer culture of Vero E6 cells in 96-well plates and incubated at 37 °C for 2 h. Virus inoculum was removed and replaced with a 0.75% methylcellulose overlay. Vero E6 cells were incubated for an additional 48 h before fixation with 4%PFA and incubated anti-flavivirus antigen, clone D1-4G2-4-15 (1:2000) (Merckmillipore, USA, MAB10216), overnight at 4 °C. Then, the cells were washed three times with PBS and incubated with FITC-conjugated anti-mouse secondary antibody (1:500) (Sigma-Aldrich, USA, F0257) for 1.5 h at room temperature. The cells were washed three times with PBS before DAPI staining.

Focus Reduction Assay for Determination of EC_{50}. Vero E6 cells were seeded in 96-well plates with 100% confluency. The cells were inoculated in triplicates with DENV2 (100 FFU/well) at 37 °C for 2 h. Then, the cells were incubated with a 0.75% methylcellulose overlay containing 0.1−1000 μM of hit compounds at 37 °C for 2 days. After the immunostaining described above, The EC_{50} values were determined by the DoseRep sigmoidal curve-fit method with OriginPro 8 (OriginLab Corporation, Northampton, MA, USA).

***In Vitro* Virus Infection Test.** Before the experiment, Vero E6 and Huh-7 were seeded in densities of 20×10^4 cells/cm^2, respectively. After 24 h of incubation under 5% CO2, 37 °C, DENV2 was inoculated to each cell culture by multiplicities of infection of 0.1 and 0.5, respectively, under serum-free culture media for 2 h. The culture plates were gently rocked every 30 min for even distribution of the virus to the cells. Hit compound solutions were prepared with a serially diluted concentration in each complete culture medium. After the incubation, the virus medium was removed and the cells were washed with sterilized PBS once, followed by the treatment of the chemical solutions. The cells were incubated under the culture chamber for 48 h. After the incubation, the cells were prepared for the immunostaining and relative viral RNA expression analysis. For the immunostaining, chemical solutions were removed and the cells were washed with sterilized PBS, followed by fixation with 4% paraformaldehyde. For the viral RNA expression analysis, the cells were treated with TRIzol after the washing process and stored at −70 °C for further analysis.

Animal Experiments. AG129 mice (129/Sv IFN-α/β, and -γ receptor deficient) were purchased from Marshall BioResources (UK). All experimental procedures were preapproved by IACUC of Seoul National University (Korea) and Jeonbuk National University (Korea) and were performed according to the guidelines of the recommendations from Association for Assessment and Accreditation of Laboratory Animal Care. As mosquitoes could transmit the DENV, the cages with filter cover were used to avoid any unexpected contact and contamination.

Mice Infection and Drug Treatment. The 10 to 12 week-old mice were administered with 300 μL of virus stock including 1×10^7 FFU of DENV2 via the intraperitoneal (IP) route. For the evaluation of antiviral efficacy of micafungin sodium (AvaChem, TX, USA, 2670S), DENV2 infected AG129 mice were administered 200 μL of micafungin sodium (75 mg/kg/day) by IP injection. Negative control (uninfected group) was administered with 300 μL PBS instead of the virus. For the drug control group, 200 μL of micafungin sodium (75 mg/kg/day) was administered solely to the non-infected AG129 mice.

Survival Rate Analysis. The mortality state was monitored daily. In the survival analysis, euthanized mice exhibiting severe disease-associated symptoms were counted as the moribund state at the moment of the exhibition.

Mouse Necropsy. At day 3 p.i., mice were sacrificed from each group ($n = 5$). Organ samples (spleen, liver, lung, small intestine, and large intestine) were collected and prepared for the virus RNA expression analysis and pathology analysis. Spleens were weighed to determine splenomegaly. For the virus RNA expression analysis, half of the spleen, liver, and lung were homogenized and treated with TRIzol reagent and stored at blow −70 °C for further analysis. The same procedures were applied to the whole samples of small intestine and large intestine. The other half of the spleen, liver, and lung were submerged to 4%PFA for fixation and stored at 4 °C.

Relative Viral RNA Expression Level Analysis. For the investigation of viral RNA expression change in the collected specimens, RNA was isolated from each cell-based and animal-based sample treated with TRIzol (Invitrogen, USA, 15596018) and quantified by a Take3 Micro-Volume plate. Using 0.1−1 μg of total RNA, cDNA was synthesized by a 5xRT-Master Mix with a random hexamer (Elpisbiotech, Korea, EBT-1511) according to the instruction manual (reaction in a 20 μL volume at 42 °C for 60 min). For target gene amplification, each primer was designed in consideration of GC content less than 50%, overlapping between two exons of the target genes with the expected amplicon size of −100 bps and PCR efficiency from 90 to 110%. Primer sequences were confirmed in the Supporting Information, Table S1. Real-time PCR was conducted to quantify viral RNA. Each reaction was conducted in a 20 μL volume with 10−100 ng of cDNA and 0.2 μM of each primer by using a POWER SYBR green PCR master mix (Applied Biosystems Inc., USA, 4367659). A 7300 Real-Time PCR System and Quantstudio3 (Applied Biosystems Inc., USA) were utilized in this study in a two-step amplification process (annealing/extension at 60 °C for 1 min and denaturation at 95 °C for 15 s) with melting curve analysis. The resulting data were analyzed by each software (SDS v1.4.1 and The QuantStudio Design & Analysis Software v1.4.3). The threshold cycle (Ct) was automatically determined. Since NTC group showed a Ct value over 36, we disposed of the result data over 36 Ct. For analysis of viremia, a linear correlative standard curve was established between log of the virus titer (FFU/mL) and the corresponding Ct value. A standard curve was derived against a serially diluted viral titer. The R^2 of standard curves was 0.9995−0.9997, and y-intercepts were determined as 39.089−43.676. The PCR efficiency was 90−102% with a 3 log linear dynamic range. According to the equation of the standard curve, the virus in plasma was calculated. For cell-based groups and mice organ samples (including whole blood), relatively quantitative viral RNA was analyzed against that of the endogenous control, GAPDH.

Pathology Analysis. Organ samples fixed with 4%PFA went through series of procedures as follows: paraffin embedding, section, and stain with hematoxylin and eosin (H&E) at the pathology core facility in the Center for Medical Innovation, Seoul National University Hospital (SNUH-CMI), Korea.

Statistical Analysis. Data plots with concentration-dependent assays were analyzed using OriginPro 8 and GraphPad Prism 7. Briefly, logarithmic sigmoidal curves were fitted according to each dataset. Error bars indicate ±SEM unless stated otherwise. Statistical significance of the *in vitro* and *in vivo* antiviral efficacy analysis was evaluated by a two-tailed t test. Statistical significance of the survival rate was analyzed by a log-rank test with R (R Foundation for Statistical Computing, Austria).

■ ASSOCIATED CONTENT

Supporting Information

The Supporting Information is available free of charge at https://pubs.acs.org/doi/10.1021/acsami.1c04641.

Experimental details including expression of the helicase recombinant protein and *in vitro* helicase assay by gel-shift (Figure S1); preparation and characterization of graphene oxide (Figure S2); comparison of spleen size

https://doi.org/10.1021/acsami.1c04641
ACS Appl. Mater. Interfaces 2021, 13, 25715−25726

(Figure S3); hematology analysis graphs (Figure S4); Kaplan−Meier analysis (Figure S5); and the sequences of primers applied in the experiments (Table S1) (PDF)

AUTHOR INFORMATION

Corresponding Author

Dal-Hee Min − *Department of Chemistry, Seoul National University, Seoul 08826, Republic of Korea; School of Biological Sciences, Seoul National University, Seoul 08826, Republic of Korea; Institute of Biotherapeutics Convergence Technology, Lemonex Inc., Seoul 06683, Republic of Korea*; Email: dalheemin@snu.ac.kr

Authors

Jungho Kim − *Department of Chemistry, Seoul National University, Seoul 08826, Republic of Korea*; orcid.org/0000-0001-7757-2427

Se-Jin Park − *Department of Chemistry, Seoul National University, Seoul 08826, Republic of Korea*

Jisang Park − *Department of Bioactive Material Sciences and Institute of Bioactive Materials, Jeonbuk National University, Jeonju 54896, Republic of Korea; Department of Molecular Biology and the Institute for Molecular Biology and Genetics, Jeonbuk National University, Jeonju 54896, Republic of Korea*

Hojeong Shin − *Department of Chemistry, Seoul National University, Seoul 08826, Republic of Korea*; orcid.org/0000-0001-5895-0955

Yong-Suk Jang − *Department of Bioactive Material Sciences and Institute of Bioactive Materials, Jeonbuk National University, Jeonju 54896, Republic of Korea; Department of Molecular Biology and the Institute for Molecular Biology and Genetics, Jeonbuk National University, Jeonju 54896, Republic of Korea*

Jae-Sung Woo − *Center for RNA Research, Institute for Basic Science (IBS), Seoul National University, Seoul 08826, Republic of Korea; Department of Life Sciences, Korea University, Seoul 02841, Republic of Korea*

Complete contact information is available at: https://pubs.acs.org/10.1021/acsami.1c04641

Author Contributions

J.K. and D.-H.M. conceived the project; J.K., S.-J.P., J.P., and H.S. performed experiments; J.K., Y.-S.J., J.-S.W., and D.-H.M. analyzed data; J.K. and D.-H.M. wrote the manuscript; D.-H.M. supervised the project.

Funding

This work was supported by the Basic Science Research Program (2016R1E1A1A01941202) through the National Research Foundation of Korea (NRF) and by Lemonex Inc. (LEMONEX-SN201901-3-30, LEMONEX-SN202003-3-60).

Notes

The authors declare the following competing financial interest(s): D.-H.M. is named on patents that describe the use of nucleic acids and carbon nanomaterials as sensors to detect nucleic acids and to measure enzyme activities. The remaining authors declare no competing interests.

ACKNOWLEDGMENTS

The authors are very grateful to Prof. J. Lescar for providing the DENV helicase plasmid and appreciate the Research Institute of Advanced Materials (RIAM) for the AFM analysis of graphene oxide.

REFERENCES

(1) Panghal, A.; Flora, S. J. S. Chapter 4 - Viral agents including threat from emerging viral infections. In *Handbook on Biological Warfare Preparedness*; Flora, S. J. S., Pachauri, V., Eds.; Academic Press: 2020; pp. 65−81.

(2) Reperant, L. A.; Osterhaus, A. D. M. E. AIDS, Avian flu, SARS, MERS, Ebola, Zika... what next? *Vaccine* **2017**, *35*, 4470−4474.

(3) Almaghaslah, D.; Kandasamy, G.; Almanasef, M.; Vasudevan, R.; Chandramohan, S. Review on the coronavirus disease (COVID-19) pandemic: its outbreak and current status. *Int. J. Clin. Pract.* **2020**, No. e13637.

(4) Corbett, K. S.; Edwards, D. K.; Leist, S. R.; Abiona, O. M.; Boyoglu-Barnum, S.; Gillespie, R. A.; Himansu, S.; Schäfer, A.; Ziwawo, C. T.; DiPiazza, A. T.; Dinnon, K. H.; Elbashir, S. M.; Shaw, C. A.; Woods, A.; Fritch, E. J.; Martinez, D. R.; Bock, K. W.; Minai, M.; Nagata, B. M.; Hutchinson, G. B.; Wu, K.; Henry, C.; Bahl, K.; Garcia-Dominguez, D.; Ma, L.; Renzi, I.; Kong, W.-P.; Schmidt, S. D.; Wang, L.; Zhang, Y.; Phung, E.; Chang, L. A.; Loomis, R. J.; Altaras, N. E.; Narayanan, E.; Metkar, M.; Presnyak, V.; Liu, C.; Louder, M. K.; Shi, W.; Leung, K.; Yang, E. S.; West, A.; Gully, K. L.; Stevens, L. J.; Wang, N.; Wrapp, D.; Doria-Rose, N. A.; Stewart-Jones, G.; Bennett, H.; Alvarado, G. S.; Nason, M. C.; Ruckwardt, T. J.; McLellan, J. S.; Denison, M. R.; Chappell, J. D.; Moore, I. N.; Morabito, K. M.; Mascola, J. R.; Baric, R. S.; Carfi, A.; Graham, B. S. SARS-CoV-2 mRNA vaccine design enabled by prototype pathogen preparedness. *Nature* **2020**, *586*, 567−571.

(5) Rodriguez-Roche, R.; Gould, E. A. Understanding the dengue viruses and progress towards their control. *Biomed Res. Int.* **2013**, *2013*, 690835.

(6) Dighe, S. N.; Ekwudu, O.; Dua, K.; Chellappan, D. K.; Katavic, P. L.; Collet, T. A. Recent update on anti-dengue drug discovery. *Eur. J. Med. Chem.* **2019**, *176*, 431−455.

(7) Rajapakse, S.; Rodrigo, C.; Rajapakse, A. Treatment of dengue fever. *Infect. Drug Resist.* **2012**, *5*, 103−112.

(8) Gan, V. C. Dengue: Moving from Current Standard of Care to State-of-the-Art Treatment. *Curr. Treat. Options Infect. Dis.* **2014**, *6*, 208−226.

(9) Lim, S. P. Dengue drug discovery: Progress, challenges and outlook. *Antiviral Res.* **2019**, *163*, 156−178.

(10) Low, J. G.; Gatsinga, R.; Vasudevan, S. G.; Sampath, A. Dengue Antiviral Development: A Continuing Journey. *Adv. Exp. Med. Biol.* **2018**, *1062*, 319−332.

(11) Ahammad, F.; Tengku Abd Rashid, T. R.; Mohamed, M.; Tanbin, S.; Ahmad Fuad, F. A. Contemporary Strategies and Current Trends in Designing Antiviral Drugs against Dengue Fever via Targeting Host-Based Approaches. *Microorganisms* **2019**, *7*, 296.

(12) Janai, H. K.; Marks, M. I.; Zaleska, M.; Stutman, H. R. Ribavirin: adverse drug reactions, 1986 to 1988. *Pediatr. Infect. Dis. J.* **1990**, *9*, 209−211.

(13) Durantel, D. Celgosivir, an alpha-glucosidase I inhibitor for the potential treatment of HCV infection. *Curr. Opin. Invest. Drugs* **2009**, *10*, 860−870.

(14) Yin, Z.; Chen, Y. L.; Schul, W.; Wang, Q. Y.; Gu, F.; Duraiswamy, J.; Kondreddi, R. R.; Niyomrattanakit, P.; Lakshminarayana, S. B.; Goh, A.; Xu, H. Y.; Liu, W.; Liu, B.; Lim, J. Y. H.; Ng, C. Y.; Qing, M.; Lim, C. C.; Yip, A.; Wang, G.; Chan, W. L.; Tan, H. P.; Lin, K.; Zhang, B.; Zou, G.; Bernard, K. A.; Garrett, C.; Beltz, K.; Dong, M.; Weaver, M.; He, H.; Pichota, A.; Dartois, V.; Keller, T. H.; Shi, P. Y. An adenosine nucleoside inhibitor of dengue virus. *Proc. Natl. Acad. Sci. U. S. A.* **2009**, *106*, 20435−20439.

(15) Hassany, S. M.; Hassan, W.; Abo-Alam, H.; Khalaf, M.; Nafeh, A. M.; Nasr-Eldin, E.; Mostafa, E. F. Direct-Acting Antiviral Drugs and Occurrence of Hepatocellular Carcinoma: Unjust or Oppressed. *Infect. Drug Resist.* **2020**, *13*, 1873−1880.

(16) Low, J. G. H.; Ooi, E. E.; Vasudevan, S. G. Current Status of Dengue Therapeutics Research and Development. *J. Infect. Dis.* **2017**, *215*, S96−S102.
(17) Kumar, R.; Harilal, S.; Gupta, S. V.; Jose, J.; Thomas Parambi, D. G.; Uddin, M. S.; Shah, M. A.; Mathew, B. Exploring the new horizons of drug repurposing: A vital tool for turning hard work into smart work. *Eur. J. Med. Chem.* **2019**, *182*, 111602.
(18) Mercorelli, B.; Palù, G.; Loregian, A. Drug Repurposing for Viral Infectious Diseases: How Far Are We? *Trends Microbiol.* **2018**, *26*, 865−876.
(19) de Oliveira, A. S.; da Silva, M. L. d.; Oliveira, A. F. C. S.; Silva, C. C. d.; Teixeira, R. R.; De Paula, S. O. NS3 and NS5 Proteins: Important Targets for Anti-Dengue Drug Design. *J. Braz. Chem. Soc.* **2014**, *25*, 1759−1769.
(20) Luo, D.; Vasudevan, S. G.; Lescar, J. The flavivirus NS2B-NS3 protease-helicase as a target for antiviral drug development. *Antiviral Res.* **2015**, *118*, 148−158.
(21) Norazharuddin, H.; Lai, N. S. Roles and Prospects of Dengue Virus Non-structural Proteins as Antiviral Targets: An Easy Digest. *Malays. J. Med. Sci.* **2018**, *25*, 6−15.
(22) Mastrangelo, E.; Pezzullo, M.; De Burghgraeve, T.; Kaptein, S.; Pastorino, B.; Dallmeier, K.; de Lamballerie, X.; Neyts, J.; Hanson, A. M.; Frick, D. N.; Bolognesi, M.; Milani, M. Ivermectin is a potent inhibitor of flavivirus replication specifically targeting NS3 helicase activity: new prospects for an old drug. *J. Antimicrob. Chemother.* **2012**, *67*, 1884−1894.
(23) Mukherjee, S.; Hanson, A. M.; Shadrick, W. R.; Ndjomou, J.; Sweeney, N. L.; Hernandez, J. J.; Bartczak, D.; Li, K.; Frankowski, K. J.; Heck, J. A.; Arnold, L. A.; Schoenen, F. J.; Frick, D. N. Identification and analysis of hepatitis C virus NS3 helicase inhibitors using nucleic acid binding assays. *Nucleic Acids Res.* **2012**, *40*, 8607−8621.
(24) Mukherjee, S.; Weiner, W. S.; Schroeder, C. E.; Simpson, D. S.; Hanson, A. M.; Sweeney, N. L.; Marvin, R. K.; Ndjomou, J.; Kolli, R.; Isailovic, D.; Schoenen, F. J.; Frick, D. N. Ebselen inhibits hepatitis C virus NS3 helicase binding to nucleic acid and prevents viral replication. *ACS Chem. Biol.* **2014**, *9*, 2393−2403.
(25) Sweeney, N. L.; Hanson, A. M.; Mukherjee, S.; Ndjomou, J.; Geiss, B. J.; Steel, J. J.; Frankowski, K. J.; Li, K.; Schoenen, F. J.; Frick, D. N. Benzothiazole and Pyrrolone Flavivirus Inhibitors Targeting the Viral Helicase. *ACS Infect. Dis.* **2015**, *1*, 140−148.
(26) Coutard, B.; Decroly, E.; Li, C.; Sharff, A.; Lescar, J.; Bricogne, G.; Barral, K. Assessment of Dengue virus helicase and methyltransferase as targets for fragment-based drug discovery. *Antiviral Res.* **2014**, *106*, 61−70.
(27) Borowski, P.; Niebuhr, A.; Mueller, O.; Bretner, M.; Felczak, K.; Kulikowski, T.; Schmitz, H. Purification and characterization of West Nile virus nucleoside triphosphatase (NTPase)/helicase: evidence for dissociation of the NTPase and helicase activities of the enzyme. *J. Virol.* **2001**, *75*, 3220−3229.
(28) Jang, H.; Kim, Y. K.; Kwon, H. M.; Yeo, W. S.; Kim, D. E.; Min, D. H. A graphene-based platform for the assay of duplex-DNA unwinding by helicase. *Angew. Chem., Int. Ed.* **2010**, *49*, 5703−5707.
(29) Jang, H.; Ryoo, S. R.; Kim, Y. K.; Yoon, S.; Kim, H.; Han, S. W.; Choi, B. S.; Kim, D. E.; Min, D. H. Discovery of hepatitis C virus NS3 helicase inhibitors by a multiplexed, high-throughput helicase activity assay based on graphene oxide. *Angew. Chem., Int. Ed.* **2013**, *52*, 2340−2344.
(30) Dumont, S.; Cheng, W.; Serebrov, V.; Beran, R. K.; Tinoco, I., Jr.; Pyle, A. M.; Bustamante, C. RNA translocation and unwinding mechanism of HCV NS3 helicase and its coordination by ATP. *Nature* **2006**, *439*, 105−108.
(31) Frick, D. N. The hepatitis C virus NS3 protein: a model RNA helicase and potential drug target. *Curr. Issues Mol. Biol.* **2007**, *9*, 1−20.
(32) Li, K.; Frankowski, K. J.; Belon, C. A.; Neuenswander, B.; Ndjomou, J.; Hanson, A. M.; Shanahan, M. A.; Schoenen, F. J.; Blagg, B. S. J.; Aube, J.; Frick, D. N. Optimization of potent hepatitis C virus NS3 helicase inhibitors isolated from the yellow dyes thioflavine S and primuline. *J. Med. Chem.* **2012**, *55*, 3319−3330.
(33) Wang, C. C.; Huang, Z. S.; Chiang, P. L.; Chen, C. T.; Wu, H. N. Analysis of the nucleoside triphosphatase, RNA triphosphatase, and unwinding activities of the helicase domain of dengue virus NS3 protein. *FEBS Lett.* **2009**, *583*, 691−696.
(34) Wu, J.; Bera, A. K.; Kuhn, R. J.; Smith, J. L. Structure of the flavivirus helicase: Implications for catalytic activity, protein interactions, and proteolytic processing. *J. Virol.* **2005**, *79*, 10268−10277.
(35) Lee, J.; Kim, J.; Kim, S.; Min, D. H. Biosensors based on graphene oxide and its biomedical application. *Adv. Drug Delivery Rev.* **2016**, *105*, 275−287.
(36) Kim, J.; Park, S. J.; Min, D. H. Emerging Approaches for Graphene Oxide Biosensor. *Anal. Chem.* **2017**, *89*, 232−248.
(37) Hummers, W. S., Jr.; Offeman, R. E. Preparation of Graphitic Oxide. *J. Am. Chem. Soc.* **1958**, *80*, 1339−1339.
(38) Zhang, J. H.; Chung, T. D. Y.; Oldenburg, K. R. A simple statistical parameter for use in evaluation and validation of high throughput screening assays. *J. Biomol. Screening* **1999**, *4*, 67−73.
(39) Schul, W.; Liu, W.; Xu, H. Y.; Flamand, M.; Vasudevan, S. G. A dengue fever viremia model in mice shows reduction in viral replication and suppression of the inflammatory response after treatment with antiviral drugs. *J. Infect. Dis.* **2007**, *195*, 665−674.
(40) Tan, G. K.; Ng, J. K. W.; Trasti, S. L.; Schul, W.; Yip, G.; Alonso, S. A non mouse-adapted dengue virus strain as a new model of severe dengue infection in AG129 mice. *PLoS Neglected Trop. Dis.* **2010**, *4*, No. e672.
(41) Park, S. J.; Kim, J.; Kang, S.; Cha, H. J.; Shin, H.; Park, J.; Jang, Y. S.; Woo, J. S.; Won, C.; Min, D. H. Discovery of direct-acting antiviral agents with a graphene-based fluorescent nanosensor. *Sci. Adv.* **2020**, *6*, No. eaaz8201.
(42) Sarathy, V. V.; White, M.; Li, L.; Gorder, S. R.; Pyles, R. B.; Campbell, G. A.; Milligan, G. N.; Bourne, N.; Barrett, A. D. T. A lethal murine infection model for dengue virus 3 in AG129 mice deficient in type I and II interferon receptors leads to systemic disease. *J. Virol.* **2015**, *89*, 1254−1266.
(43) Barth, O. M.; Barreto, D. F.; Paes, M. V.; Takiya, C. M.; Pinhao, A. T.; Schatzmayr, H. G. Morphological studies in a model for dengue-2 virus infection in mice. *Mem. Inst. Oswaldo Cruz* **2006**, *101*, 905−915.
(44) Barreto, D. F.; Takiya, C. M.; Schatzmayr, H. G.; Nogueira, R. M. R.; da Costa Farias-Filho, J.; Barth, O. M. Histopathological and ultrastructural aspects of mice lungs experimentally infected with dengue virus serotype 2. *Mem. Inst. Oswaldo Cruz* **2007**, *102*, 175−182.
(45) Sarathy, V. V.; White, M.; Li, L.; Kaiser, J. A.; Campbell, G. A.; Milligan, G. N.; Bourne, N.; Barrett, A. D. T. Characterization of a murine model of non-lethal, symptomatic dengue virus infection. *Sci. Rep.* **2018**, *8*, 4900.
(46) Basavannacharya, C.; Vasudevan, S. G. Suramin inhibits helicase activity of NS3 protein of dengue virus in a fluorescence-based high throughput assay format. *Biochem. Biophys. Res. Commun.* **2014**, *453*, 539−544.
(47) Odds, F. C.; Brown, A. J. P.; Gow, N. A. R. Antifungal agents: mechanisms of action. *Trends Microbiol.* **2003**, *11*, 272−279.
(48) Kim, C.; Kang, H.; Kim, D. E.; Song, J. H.; Choi, M.; Kang, M.; Lee, K.; Kim, H. S.; Shin, J. S.; Jeong, H.; Jung, S.; Han, S. B.; Kim, J. H.; Ko, H. J.; Lee, C. K.; Kim, M.; Cho, S. Antiviral activity of micafungin against enterovirus 71. *Virol. J.* **2016**, *13*, 99.
(49) Ho, Y. J.; Liu, F. C.; Yeh, C. T.; Yang, C. M.; Lin, C. C.; Lin, T. Y.; Hsieh, P. S.; Hu, M. K.; Gong, Z.; Lu, J. W. Micafungin is a novel anti-viral agent of chikungunya virus through multiple mechanisms. *Antiviral Res.* **2018**, *159*, 134−142.
(50) Nanri, T.; Iwanaga, E.; Fujie, S.; Yamada, Y.; Horikawa, K.; Mitsuya, H.; Asou, N. Micafungin-induced immune hemolysis attacks. *Int. J. Hematol.* **2009**, *89*, 139−141.

https://doi.org/10.1021/acsami.1c04641
ACS Appl. Mater. Interfaces 2021, 13, 25715−25726

(51) Peter, T.; Bissinger, R.; Signoretto, E.; Mack, A. F.; Lang, F. Micafungin-Induced Suicidal Erythrocyte Death. *Cell. Physiol. Biochem.* **2016**, *39*, 584−595.
(52) Pozo, A. L.; Godfrey, E. M.; Bowles, K. M. Splenomegaly: investigation, diagnosis and management. *Blood Rev.* **2009**, *23*, 105−111.
(53) Bronte, V.; Pittet, M. J. The spleen in local and systemic regulation of immunity. *Immunity* **2013**, *39*, 806−818.
(54) Chapman, J.; Bansal, P.; Goyal, A.; Azevedo, A. M. *Splenomegaly*; StatPearls: Treasure Island (FL), 2020.
(55) Fuchs, B. B.; Li, Y.; Li, D.; Johnston, T.; Hendricks, G.; Li, G.; Rajamuthiah, R.; Mylonakis, E. Micafungin Elicits an Immunomodulatory Effect in Galleria mellonella and Mice. *Mycopathologia* **2016**, *181*, 17−25.
(56) Vaughn, D. W.; Green, S.; Kalayanarooj, S.; Innis, B. L.; Nimmannitya, S.; Suntayakorn, S.; Endy, T. P.; Raengsakulrach, B.; Rothman, A. L.; Ennis, F. A.; Nisalak, A. Dengue viremia titer, antibody response pattern, and virus serotype correlate with disease severity. *J. Infect. Dis.* **2000**, *181*, 2−9.
(57) Libraty, D. H.; Endy, T. P.; Houng, H.-S. H.; Green, S.; Kalayanarooj, S.; Suntayakorn, S.; Chansiriwongs, W.; Vaughn, D. W.; Nisalak, A.; Ennis, F. A.; Rothman, A. L. Differing influences of virus burden and immune activation on disease severity in secondary dengue-3 virus infections. *J. Infect. Dis.* **2002**, *185*, 1213−1221.
(58) Sehrawat, P.; Biswas, A.; Kumar, P.; Singla, P.; Wig, N.; Dar, L.; Sood, R. Role of Cytokines as Molecular Marker of Dengue Severity. *Mediterr. J. Hematol. Infect. Dis.* **2018**, *10*, No. e2018023.
(59) Kwong, A. D.; Rao, B. G.; Jeang, K. T. Viral and cellular RNA helicases as antiviral targets. *Nat. Rev. Drug Discovery* **2005**, *4*, 845−853.
(60) Biswas, S.; Sukla, S.; Field, H. J. Helicase-primase inhibitors for herpes simplex virus: looking to the future of non-nucleoside inhibitors for treating herpes virus infections. *Future Med. Chem.* **2014**, *6*, 45−55.
(61) Wald, A.; Corey, L.; Timmler, B.; Magaret, A.; Warren, T.; Tyring, S.; Johnston, C.; Kriesel, J.; Fife, K.; Galitz, L.; Stoelben, S.; Huang, M. L.; Selke, S.; Stobernack, H. P.; Ruebsamen-Schaeff, H.; Birkmann, A. Helicase-primase inhibitor pritelivir for HSV-2 infection. *N. Engl. J. Med.* **2014**, *370*, 201−210.
(62) Chen, Y. L.; Yin, Z.; Duraiswamy, J.; Schul, W.; Lim, C. C.; Liu, B.; Xu, H. Y.; Qing, M.; Yip, A.; Wang, G.; Chan, W. L.; Tan, H. P.; Lo, M.; Liung, S.; Kondreddi, R. R.; Rao, R.; Gu, H.; He, H.; Keller, T. H.; Shi, P. Y. Inhibition of dengue virus RNA synthesis by an adenosine nucleoside. *Antimicrob. Agents Chemother.* **2010**, *54*, 2932−2939.
(63) Gumbo, T.; Drusano, G. L.; Liu, W.; Kulawy, R. W.; Fregeau, C.; Hsu, V.; Louie, A. Once-weekly micafungin therapy is as effective as daily therapy for disseminated candidiasis in mice with persistent neutropenia. *Antimicrob. Agents Chemother.* **2007**, *51*, 968−974.

https://doi.org/10.1021/acsami.1c04641
ACS Appl. Mater. Interfaces 2021, 13, 25715−25726